Abstract

In the Kane silicon-based electron-mediated nuclear spin quantum computer architecture, phosphorous is doped at precise positions in a silicon lattice, and the P donor nuclear spins act as qubits. Logical operations on the nuclear spins are performed using externally applied magnetic and electric fields. There are two important interactions: the hyperfine and exchange interactions, crucial for logical qubit operations. Single qubit operations are performed by applying radio frequency magnetic fields resonant with targeted nuclear spin transition frequencies, tuned by the gate-controlled hyperfine interaction. Two qubit operations are mediated through the exchange interaction between adjacent donor electrons. It is important to examine how these two interactions vary as functions of experimental parameters. Here we provide such an investigation. First, we examine the effects of varying several experimental parameters: gate voltage, inter donor separation, donor depth below the silicon oxide interface and back gate depth, to explore how these variables affect the donor electro density. Second, we calculate the hyperfine interaction and the exchange coupling as a function of these parameters. These calculations were performed using an anisotropic effective mass Hamiltonian. The electric field potential was obtained using Technology Computer Aided Design software, and the interfaces were modelled as a barrier using a step function. We aim to provide relevant information for the experimental design of these devices and highlight the significance of environmental factors other than gate potential that affect the donor electron.

Device modelling for the Kane quantum computer architecture: solution of the donor electron Schrödinger equation.

Louise M. Kettle, Hsi-Sheng Goan, Sean C. Smith, Cameron J. Wellard and Lloyd C.L. Hollenberg.

February 27, 2004

1 Introduction

Advances in quantum error correction codes and quantum algorithms which outperform their best known classical counterparts, have prompted a search for a scalable quantum computer. Recently, several designs for silicon-based solid state quantum computers have been proposed.[2, 3, 4, 5, 6, 7] The theoretical study presented here is relevant to these silicon-based quantum computer architectures, as it provides information about both the electron wave function and nuclear spin of the ^{31}P donors.

Donor nuclear and electronic spins are promising candidates for solid state spin qubits because of their long coherence times. The solid-state nuclear spin quantum computer proposed by Kane[1] uses a qubit array of nuclear spins of ^{31}P dopants embedded within a silicon crystal matrix. This model is based on the use of ^{31}P nuclear spins as qubits as it has a nuclear spin of 1/2, implanted in isotopically pure ^{28}Si which has a nuclear spin of 0.

In this work we concentrate our efforts on the Kane model,[1] in which the P nuclear spin acts as a qubit with the donor electron functioning to meditate control of single qubit operations and interaction between individual qubits, and permit read-out of nuclear spin states. Perturbing the electron density with externally applied electric and magnetic fields is crucial in controlling logical operations at individual qubits. Logical operations on the qubits are performed by varying the electrostatic potential at surface electrodes above the qubits (A-gates), and between qubits (J-gates).

The A-gate tunes the resonance frequency of individual spins, and single qubit operations are performed using a globally applied RF magnetic field that rotates targeted nuclear spins at resonance. The J-gate controls the electron-electron exchange interaction between adjacent qubits. In order to correctly specify fabrication

parameters it is necessary to predict the strength of the hyperfine interaction between the nuclear spin and the electron spin, and also the exchange interaction between two donor electrons as a function of donor separation, donor depth and surface gate configuration and voltage.

Application of a potential to an A-gate perturbs the electron density of the donor electron, thereby varying the hyperfine interaction between the nuclear qubit and its donor electron. Similarly applying a potential at the J-gate perturbs the two adjacent donor electron wave functions, inducing an electron-mediated nuclear spin exchange coupling to occur which allows adjacent qubits to interact. Both these interactions require us to know the P donor electron wave function in the Si lattice in the presence of the externally applied electric field, and the interface regions.

Considerable developments in the theory have been made since Kohn and Luttinger's [11, 12] original work, where they calculated the P donor ground state in bulk Si variationally, using a single trial wave function. Several authors [13, 14, 15] have kept the Si Bloch states expansions in their calculations which reveals the underlying oscillating behaviour of the donor electron in the Si lattice. Koiller *et al.*[14, 15] studied the exchange coupling between a donor pair also in bulk Si, and in the absence of an electric field. In their calculations they used an effective mass theory in which the expansion of the ground state donor electron wave function includes the Bloch states of the six conduction band minima. They approximated the coefficients of the Bloch functions and used an anisotropic Kohn-Luttinger variational form for the envelope wave function. Wellard *et al.*[13] have extended these calculations to remove some of their approximations. They obtained the donor electron wave function and exchange coupling with an applied J-gate bias, in order to study the fast exchange oscillations with respect to fabrication strategies. Several authors[14, 16, 17] have investigated the effects induced by strain and interface regions on donor states. These external influences partially lift the valley degeneracy in the bulk silicon.

Other authors (including this work) have concentrated their efforts into modelling the donor electron "envelope" wave function, to gain more insight into the overall behaviour of the donor electron influenced by an electric field and the boundary effects of the Si/SiO_2 barrier.

The effect of an electric field potential at a gate above a P donor in a silicon substrate on the hyperfine coupling between the P donor electron and nucleus, has already been reported by several authors. Kane [18] and Larinov *et al.* [19] calculate the effect of an electric field potential in the bulk silicon host using perturbative theory, excluding the additional interface potentials. Wellard *et al.*[20] consider both the influence of the electric field and interface barriers on the contact hyperfine coupling, using an isotropic effective mass Hamiltonian.

Smit *et al.*[21] modelled the effect of a gate nearby the donor electron using an isotropic effective mass approach, and expand the wave function as a linear combination of Gaussians. Similarly to our work, they found that depending on

the separation of the dopant and the gate, the electron transfer is either gradual or abrupt.

The donor electron exchange coupling as a function of gate voltage has also been investigated using a variety of methods. Fang *et al.*[22] calculated the donor electron wave function using an isotropic effective mass approximation. They modeled the J-gate potential qualitatively as a 1-D parabolic well with its minimum located in the middle of the two donor sites, but did not consider the boundary effects of the silicon host geometry in their calculation. In their work they used an unrestricted Hartree-Fock method with a generalised valence bond wave function to study the two-electron system and calculate the exchange coupling. Parisoli *et al.*[23] have calculated the effect of the J-gate potential, interface regions and donor separation using an isotropic effective mass Hamiltonian. We extended this work to include the anisotropy of the effective masses in Si into the Hamiltonian.

In this work we provide a numerical study of hydrogenic effective mass theory for a P impurity atom in Si in the presence of an electric field and interfaces. We examine the effects of varying several experimental parameters in the Kane quantum computer architecture: gate voltage, donor depth below the silicon oxide layer, inter donor separation and back gate depth. We aim to provide relevant information for the experimental design of these devices. Our approach allows us to calculate the smooth donor-modulated envelope function relatively quickly, to achieve quantitatively reasonable results. This allows us to explore a greater range of device parameters than methods which include the underlying Bloch structure, as the calculations are not as computationally expensive.

We first calculated the single donor electron wave function variationally in zero field, using an effective anisotropic mass Hamiltonian. The contribution of the Si lattice is accounted for by considering it as a uniform dielectric medium and using the anisotropic effective masses around a single conduction band minimum. The P nucleus impurity potential was modelled as a screened Coulombic potential. We expanded the donor electron wave function in a basis of deformed hydrogenic functions, following Faulkner's approach.[8] The Hamiltonian was then diagonalised with the ground state energy minimised by varying the Bohr radii in the basis functions.

This approach was then extended to include the effects of an electrostatic potential at either the A or J-gate and the interface regions, and this new Hamiltonian was diagonalised. Once the donor electron wave function was obtained we then calculated the contact hyperfine interaction and the electron-electron exchange interaction, at the varying device parameters.[9, 10] The exchange coupling was calculated using Heitler-London theory, which models the donor pair wave function as the symmetrised and anti-symmetrised product of the two single donor electron wave functions at each P atom.

Because we use a single valley anisotropic effective mass approach to calculate the donor wave function in the Si wafer device, the effective Bohr radii are fixed in

our co-ordinate system. We optimise the donor electron energy with respect to the effective Bohr radii, by choosing the smaller effective Bohr radius in the direction perpendicular to the interface regions, and the larger ones in the direction parallel to the interfaces. This means that our calculations for the exchange coupling are higher than other reported values, [13, 14, 15, 23] because we chose the larger Bohr radius also to be along the inter donor axis. We are extending these calculations using a more refined approach that includes the effects of all six conduction band minima, to see how the electric field influences the multi-valley donor electron wave function.

In section 2 and 3 we will discuss some background effective mass theory, and the approximations inherent in the method we use to model the P donor wave function. Section 4 discusses the approach we took to obtain the phosphorus donor ground state in bulk silicon in zero field. We outline the method we used to model a voltage at the A or J-gate, and the interface regions in section 5. In section 6 we discuss how we calculated both the exchange and hyperfine interaction. The numerical results using the methods outlined in the previous sections are presented in section 7 and 8, for an applied A and J-gate voltage respectively. Finally we summarise our major findings in section 9.

We found that all the device parameters modelled in this work become crucial factors in determining the strength of both the hyperfine and exchange interactions. The proximity of the qubit to the gate and the silicon oxide layer is very important in determining the degree to which the donor electron density can be perturbed by the gate. We have found that as the donor is displaced further from the gate, the electron transfer proceeds from gradual transference to the gate, to an abrupt process whereby the electron is ionised to the gate for large enough positive voltages.

2 Background

In the silicon valence bond network the P atom replaces a Si atom and forms four covalent bonds tetrahedrally in the lattice. As P has an extra proton and electron than Si, it is a donor. We expect the P atom to act effectively like a hydrogen atom with its one donor electron, but with its nuclear charge screened by the crystal core electrons. So a rough calculation in this framework is to treat the silicon substrate as a uniform dielectric, with dielectric constant, ϵ, and ignore crystal effects. The Hamiltonian for the P donor electron is equivalent to the Hamiltonian for the the hydrogen atom with scaled units:

$$H = \frac{-\hbar^2}{2m_*}\nabla^2 - \frac{e^2}{\epsilon r},$$

where $\epsilon = 11.4$ is the static dielectric constant, and $m_* \approx m_\perp = 0.1905 m_0$ where m_0 is mass of free electron. In these scaled units, the Bohr radius becomes $a = 31.7\dot{A}$

and ground state energy, $E = -19.88$meV. Experimentally the ground state energy is -45meV.

A more rigorous derivation of effective mass theory is needed to improve on these results and adequately describe the donor electron wave function, to include the effects of the crystal.

3 Effective Mass Theory

The Hamiltonian for the donor electron wave function is:

$$\left(H^0 + U(r)\right)\Psi(\mathbf{r}) = E\Psi(\mathbf{r}), \tag{1}$$

where H^0 is Hamiltonian for the perfect crystal Si, and $U(r)$ is the impurity potential.

Now we expand $\Psi(\mathbf{r})$ as a sum of the perfect crystal Si Bloch functions, $\psi^0_{nk}(\mathbf{r})$, (here the superscript 0 will always refer to the silicon Bloch wave functions, ψ^0_{nk} and energies, E^0_{nk}):

$$\Psi(\mathbf{r}) \quad = \quad \sum_{n,k} F_{nk}\psi^0_{nk}(\mathbf{r}).$$

Here the index $\mathbf{k}$ is summation over all wave vectors, in the first Brillouin zone and the index n enumerates the energy bands at the same $\mathbf{k}$. Here ψ^0_{nk} satisfy: $H^0\psi^0_{nk} = E^0_{nk}\psi^0_{nk}$.

So now (1) becomes:

$$F_{nk}E^0_{nk} + \sum_{n'k'} F_{n'k'}\langle\psi^0_{nk}|U(r)|\psi^0_{n'k'}\rangle \quad = \quad F_{nk}E. \tag{2}$$

The Bloch functions ψ^0_{nk} have a certain form given by Bloch's theorem, which states that solutions of Schrödinger's equation for a periodic potential have the form:[24]

$$\psi^0_{nk}(\mathbf{r}) \quad = \quad e^{i\mathbf{k}.\mathbf{r}}u_{nk}(\mathbf{r}),$$

where $u_{nk}(\mathbf{r})$ has the same period as the translational period of the crystal $\mathbf{R}$, ie. $u_{nk}(\mathbf{r}) = u_{nk}(\mathbf{r} + \mathbf{R})$. To satisfy this periodicity condition we can let

$$u_{nk}(\mathbf{r}) \quad = \quad \sum_{\mathbf{G}} A_{nk}(\mathbf{G})e^{i\mathbf{G}.\mathbf{r}},$$

where $\mathbf{G}$ is any reciprocal lattice vector which satisfies $e^{i\mathbf{G}.\mathbf{R}} = 1$.

We can now express the integral in (2) as:

$$\langle\psi^0_{nk}|U(r)|\psi^0_{n'k'}\rangle \quad = \quad \sum_{\mathbf{G}} C^{kk'}_{nn'}(\mathbf{G}) \int d\mathbf{r}U(r)e^{i(\mathbf{G}+\mathbf{k}'-\mathbf{k}).\mathbf{r}},$$

$$
\begin{aligned}
&= \sum_{\mathbf{G}} C^{kk'}_{nn'}(\mathbf{G})\overline{U}(\mathbf{k}-\mathbf{k}'-\mathbf{G}),\\
\text{where } \overline{U}(\mathbf{q}) &= \int d\mathbf{r} U(r) e^{-i\mathbf{q}.\mathbf{r}},\\
\text{and } C^{kk'}_{nn'}(\mathbf{G}) &= \sum_{\mathbf{G}'} A^{*}_{nk}(\mathbf{G}'-\mathbf{G}) A_{n'k'}(\mathbf{G}'),
\end{aligned}
$$

and (2) becomes:

$$
F_{nk}E^0_{nk} + \sum_{n'k'} F_{n'k'} \sum_{\mathbf{G}} C^{kk'}_{nn'}(\mathbf{G})\overline{U}(\mathbf{k}-\mathbf{k}'-\mathbf{G}) \quad = \quad F_{nk}E. \tag{3}
$$

Equation (3) is still exact and we need to solve (3) to find the eigenvector coefficients F_{nk} and eigenvalues E.

To solve (3) we make several approximations. The first approximation is to assume the extra electron on phosphorous will fill (or lie close to) the next available energy level in the silicon lattice band structure. The next available energy level in silicon is its conduction band minima. Silicon is a semiconductor so its valence bands are completely filled and there is an indirect energy gap of approximately 1eV to the conduction band minima. The band structure of silicon has 6 equivalent conduction band minima along the 6 crystallographic axes, at wave vectors $\mathbf{k_i} = (\pm 0.85, 0, 0), (0, \pm 0.85, 0), (0, 0, \pm 0.85)$ in units of $2\pi/a^o$, where a^o is the Si lattice primitive cell length. Experimentally the ground state energy of P is found to be -45meV below the conduction band minima, so P is a shallow donor and this approximation is quite good. This assumption means the index n summing over all bands can be dropped, and (3) becomes:

$$
F_k E^0_k + \sum_{k'} F_{k'} \sum_{\mathbf{G}} C_{kk'}(\mathbf{G})\overline{U}(\mathbf{k}-\mathbf{k}'-\mathbf{G}) \quad = \quad F_k E. \tag{4}
$$

In Kohn-Luttinger effective mass theory we drop the $\mathbf{G} \neq 0$ terms and use $C_{kk'}(\mathbf{0}) \approx 1$ and get:

$$
F_k E^0_k + \sum_{k'} F_{k'}\overline{U}(\mathbf{k}-\mathbf{k}') \quad = \quad F_k E. \tag{5}
$$

This approximation is only valid if:

$$
\frac{\sum_{\mathbf{G}\neq 0} C_{kk'}(\mathbf{G})\overline{U}(\mathbf{k}-\mathbf{k}'-\mathbf{G})}{\overline{U}(\mathbf{k}-\mathbf{k}')} \quad << \quad 1.
$$

If $U(r)$ has no strong high Fourier components then this requirement is well-satisfied. As we assume the impurity potential takes the form of a screened Coulombic potential, it fulfills this requirement as it is a smooth potential, slowly varying with r. In the region of the core this assumption breaks down as the donor electron is no longer screened by the crystal core electrons, and $U(r)$ does not account for the repulsion between the donor electron and the crystal core electrons.

To solve (5) we anticipate solutions for which F_k is localized about the 6 equivalent conduction band minima:

$$F_k \quad = \quad \sum_{i=1}^{6} \alpha_i F_i(\mathbf{k}).$$

We expand the energy , E_k^0, about the conduction band minima, $\mathbf{k_i} = (0, 0, 0.85)\frac{2\pi}{a^o}$, (along the z-axis for example) as:

$$E_{k_i}^0 \quad = \quad \frac{\hbar^2}{2}\left(\frac{k_x^2 + k_y^2}{m_\perp} + \frac{(k_z - k_i)^2}{m_\parallel}\right),$$

where $m_\perp = 0.1905 m_0$ and $m_\parallel = 0.9163 m_0$ are the transverse and longitudinal effective masses respectively, and m_0 is the mass of a free electron.

Using these approximations we re-evaluate equation (5), and multiply (5) by $e^{i\mathbf{k}.\mathbf{r}}$ and sum over $\mathbf{k}$. This gives:

$$\begin{aligned} \sum_{i=1}^{6} \alpha_i e^{i\mathbf{k_i}.\mathbf{r}}[T_i(-i\nabla) + U(r) - E]F_i(r) \quad &= \quad 0, \qquad (6) \\ \text{where } F_i(r) \quad &= \quad \sum_{\mathbf{k}} F_i(\mathbf{k}) e^{i(\mathbf{k}-\mathbf{k_i}).\mathbf{r}}, \\ \text{and } T_1(-i\nabla) \quad &\equiv \quad \frac{\hbar^2}{2m_\perp}\left(\frac{\partial^2}{\partial_x^2} + \frac{\partial^2}{\partial_y^2}\right) + \frac{\hbar^2}{2m_\parallel}\frac{\partial^2}{\partial_z^2}, \text{ etc.} \end{aligned}$$

We solved (6) using two methods. In the first approach we followed the method of Pantelides and Sah,[25, 26] and solved (6) variationally. Here we kept all 6 valley terms in the equation, but used the spherical approximation for the energies, $E_{k_i}^0$:

$$E_{k_i}^0 \quad \approx \quad \frac{\hbar^2}{2m_*}(k_x^2 + k_y^2 + (k_z - k_i)^2), \text{ in the spherical band approximation,}$$

where $m_* \approx 0.29 m_0$ is the spherically averaged effective mass. We expanded the donor "envelope" function, $F_i(r)$, as a sum of the isotropic $1s$ and $2s$ hydrogenic orbitals. We varied the Bohr radius a in these two functions to minimise the ground state energy. Variationally solving (6) gave $a = 9.28$Å and $E(a) = -48.7$meV using both trial functions, and $a = 11.27$Å and $E(a) = -46.9$meV using just the $1s$ trial function.

When we want to introduce the electric field and Si host geometry potentials into the Hamiltonian this method is limited, because the basis we are using is too small to describe large perturbations in the donor electron wave function. For this reason we concentrated our efforts on the next method: single valley effective mass theory.

In this approach we consider only a single conduction band minima to reduce the complexity of the calculations, but the expansion for E_k^0 does include the full

anisotropy of the effective masses. We follow Faulkner's[8] method to obtain the zero field donor electron ground state using a basis of deformed hydrogenic orbitals. This method is advantageous because we expand the donor wave function in a large basis which has the flexibility to deform with the applied field and Si host geometry.

In this work we model electrostatic gate operations in the Kane quantum computer. We use a Hamiltonian for the donor electron which includes the anisotropy of the effective masses in the silicon host, the electric field potential and the interface regions in the Si wafer device. We calculate the contact hyperfine interaction and exchange coupling as a function of the varying experimental parameters: qubit separation, qubit depth, gate voltage and back gate depth. We aim to provide relevant information for experimental engineering of these devices and highlight the significance of environmental factors other than the gate potential which may perturb the donor electron wave function.

4 Faulkner's Method

We neglect the inter valley coupling terms in equation (6), which results in the zero field single valley effective mass equation for P in Si:

$$-\left(\frac{\hbar^2}{2m_\perp}\left(\frac{\partial^2}{\partial x^2}+\frac{\partial^2}{\partial y^2}\right)+\frac{\hbar^2}{2m_{||}}\frac{\partial^2}{\partial z^2}+\frac{e^2}{\epsilon r}\right)\Psi(\mathbf{r}) \quad = \quad E\Psi(\mathbf{r}). \tag{7}$$

Here $\Psi(\mathbf{r})$ is the donor electron envelope wave function. This equation is very successful in reproducing the donor excited states, where the inter valley mixing is negligible. Here we are expanding the energy, E_k^0 around the conduction band minima along the z-axis at $\mathbf{k}=(0,0,k_i)$:

$$E_k^0 \quad = \quad E_0^0+\frac{\hbar^2}{2m_\perp}\left(k_x^2+k_y^2\right)+\frac{\hbar^2}{2m_{||}}\left(k_z^2-k_i^2\right).$$

If we use atomic units, where the unit of length $a_B=\hbar^2\epsilon/m_\perp e^2=31.667\dot{A}$ and unit of energy $E_B=m_\perp e^4/2\hbar^2\epsilon^2=19.9436$meV, equation (7) becomes:

$$-\left(\frac{\partial^2}{\partial x^2}+\frac{\partial^2}{\partial y^2}+\gamma\frac{\partial^2}{\partial z^2}+\frac{2}{r}\right)\Psi(\mathbf{r}) \quad = \quad E\Psi(\mathbf{r}), \tag{8}$$

where $\gamma=m_\perp/m_{||}=0.2079$.

We expand $\Psi(\mathbf{r})$ using an orthonormal basis set consisting of deformed hydrogenic orbitals, $\phi_{nlm}(x,y,z,a,\beta)$, where a is the Bohr radius in the x,y directions, and β an adjustable parameter which gives Bohr radius b in z direction for the deformed hydrogen orbitals.

$$\Psi(x,y,z,a,\beta) \quad = \quad \sum_{n,l,m}\phi_{nlm}(x,y,z,a,\beta),$$

$$\text{where } \phi_{nlm}(x,y,z,a,\beta) \;=\; \left(\frac{\beta}{\gamma}\right)^{1/4} \psi_{nlm}(x,y,\left(\frac{\beta}{\gamma}\right)^{1/2} z,a).$$

$\psi_{nlm}(x,y,z,a)$ are the normalized hydrogenic wave functions:

$$\begin{aligned}
\psi_{nlm}(x,y,z,a) &= R_{nl}(a,r)Y_l^m(\theta,\phi),\\
\text{where } R_{nl}(a,r) &= A_{nl}^a r^l e^{-r/an} \sum_{s=0}^{n-l-1} b_{snl}^a r^s,\\
\text{and} \qquad A_{nl}^a &= \frac{2}{a^{3/2}n^2}\left(\frac{(n-l-1)!}{((n+l)!)^3}\right)^{1/2}\left(\frac{2}{an}\right)^l,\\
b_{snl}^a &= (-1)^s \frac{((n+l)!)^2}{(n-l-s-1)!(2l+s+1)!s!}\left(\frac{2}{an}\right)^s,
\end{aligned}$$

and for $m \geq 0$:

$$\begin{aligned}
Y_l^m(\theta,\phi) &= (-1)^m Q_{lm} P_l^{|m|}(\cos\theta)e^{im\phi},\\
Y_l^{-m}(\theta,\phi) &= (-1)^m Y_l^{m*}(\theta,\phi),\\
&= Q_{lm} P_l^{|m|}(\cos\theta)e^{-im\phi},
\end{aligned}$$

where:

$$Q_{lm} = \left(\frac{2l+1}{4\pi}\frac{(l-|m|)!}{(l+|m|)!}\right)^{1/2},$$

and P_μ^ν are associated Legendre functions of degree μ and order ν. [30, 8, 27]

Using the deformed hydrogenic basis, we write the Hamiltonian matrix elements as:

$$\begin{aligned}
&\langle\phi_{n'l'm'}|H_0|\phi_{nlm}\rangle\\
&= \sqrt{\frac{\beta}{\gamma}}\int dx^3 \psi^*_{n'l'm'}(x,y,\sqrt{\frac{\beta}{\gamma}}z,a)\Big[-\frac{\partial^2}{\partial x^2}-\frac{\partial^2}{\partial y^2}-\gamma\frac{\partial^2}{\partial z^2}-\frac{2}{r}\Big]\psi_{nlm}(x,y,\sqrt{\frac{\beta}{\gamma}}z,a).
\end{aligned} \tag{9}$$

Now we make a change of variable: $z = \sqrt{\beta/\gamma}z$ and equation (9) becomes:

$$\begin{aligned}
&\langle\phi_{n'l'm'}|H_0|\phi_{nlm}\rangle\\
&= \int dx^3 \psi^*_{n'l'm'}(x,y,z,a)\Big[-\frac{\partial^2}{\partial x^2}-\frac{\partial^2}{\partial y^2}-\beta\frac{\partial^2}{\partial z^2}-\frac{2}{\sqrt{x^2+y^2+(\gamma/\beta)z^2}}\Big]\psi_{nlm}(x,y,z,a),\\
&= \int dx^3 \psi^*_{n'l'm'}\Big[-\nabla^2+(1-\beta)\frac{\partial^2}{\partial z^2}-\frac{2}{\sqrt{x^2+y^2+(\gamma/\beta)z^2}}\Big]\psi_{nlm}.
\end{aligned} \tag{10}$$

Now using $(-\nabla^2 - 2/ar)\psi_{nlm} = -(1/a^2n^2)\psi_{nlm}$, the first term in equation (10) becomes:

$$\begin{aligned}\int dx^3 \psi^*_{n'l'm'}\left(-\nabla^2\psi_{nlm}\right) &= \delta_{nn'}\delta_{ll'}\delta_{mm'}\frac{-1}{a^2n^2} + \delta_{ll'}\delta_{mm'}\frac{2}{a}\int dr R_{n'l}(a,r)R_{nl}(a,r)\times r,\\ &= \delta_{nn'}\delta_{ll'}\delta_{mm'}\frac{-1}{a^2n^2} + \delta_{ll'}\delta_{mm'}\frac{2}{a}J^{(1)}(n,n',l,l,a),\end{aligned}$$

where:

$$J^{(k)}(n,n',l,l',a) = \int_0^\infty dr R_{n'l'}(a,r)R_{nl}(a,r)\times r^k.$$

The third term in equation (10) was evaluated numerically after the following simplifications were made:

$$\begin{aligned}&-2\int dx^3 \frac{\psi^*_{n'l'm'}\psi_{nlm}}{\sqrt{x^2+y^2+(\gamma/\beta)z^2}}\\ &= -2J^{(1)}(n,n',l,l,a)\int d\Omega \frac{Y^*_{l'm'}Y_{lm}}{\sqrt{1-(1-\gamma/\beta)\cos^2\theta)}}.\end{aligned}$$

If we let the integral over the angular part be $I(l,l',m,m')$ we have:

$$\begin{aligned}I(l,l',m,m') &= \int d\Omega \frac{Y^*_{l'm'}Y_{lm}}{\sqrt{1-(1-\gamma/\beta)\cos^2\theta)}} \qquad (11)\\ &= (-1)^{m+m'}Q_{l'm'}Q_{lm}\int_0^{2\pi} d\phi e^{i(m-m')\phi}\int_0^\pi d\theta \frac{\sin\theta P_{l'}^{|m'|}(\cos\theta)P_l^{|m|}(\cos\theta)}{\sqrt{1-(1-\gamma/\beta)\cos^2\theta)}}.\end{aligned}$$

We let $u = \cos\theta$, then equation (11) becomes:

$$I(l,l',m) = -\delta_{mm'}(-1)^{m+m'}Q_{l'm'}Q_{lm}\int_1^{-1} du \frac{P_{l'}^{|m'|}(u)P_l^{|m|}(u)}{\sqrt{1-(1-\gamma/\beta)u^2)}}.$$

Now $P_l^{|m|}(u)$ is an even function if $l+l'$ is even, and an odd function if $l+l'$ is odd, so $I(l,l',m)$ is zero for $l+l'$ odd. So for $l+l'$ even, the integral for $I(l,l',m)$ becomes:

$$I(l,l',m) = 2\delta_{mm'}Q_{l'm}Q_{lm}\int_0^1 du \frac{P_{l'}^{|m|}(u)P_l^{|m|}(u)}{\sqrt{1-(1-\gamma/\beta)u^2)}}.$$

The second term in equation (10) was given by Faulkner, [8] and the Hamiltonian matrix, H_0, becomes:

for $l' = l$, $m' = m$:
$\langle\phi_{n'lm}|H_0|\phi_{nlm}\rangle$

$$= -2I(l,l,m)J^{(1)}(n,n',l,l,a) + \left(1-(1-\beta)\frac{1}{3}\left[1+\frac{2l(l+1)-6m^2}{(2l-1)(2l+3)}\right]\right)$$
$$\times\left(-\delta_{nn'}\frac{1}{a^2n^2}+\frac{2}{a}J^{(1)}(n,n',l,l,a)\right),$$

for $l'=l-2,\ m'=m$:

$\langle\phi_{n'(l-2)m}|H_0|\phi_{nlm}\rangle$

$$= -2I(l,l-2,m)J^{(1)}(n,n',l,l-2,a) + (1-\beta)\frac{1}{(2l-1)}\left(\frac{(l^2-m^2)[(l-1)^2-m^2]}{(2l+1)(2l-3)}\right)^{1/2}$$
$$\times\left\{\frac{1}{2a^2}\left(\frac{1}{n^2}+\frac{1}{n'^2}\right)J^{(2)}(n,n',l,l-2,a) + (2l-1)D^{(1)}(n,n',l,l-2,a)\right.$$
$$\left.-\frac{2}{a}J^{(1)}(n,n',l,l-2,a) + l(2l-1)J^{(0)}(n,n',l,l-2,a)\right\},$$

for $l'=l\pm 2j,\ j\neq 0,1,\ m'=m$:

$\langle\phi_{n'(l\pm 2j)m}|H_0|\phi_{nlm}\rangle$

$$= -2I(l,l\pm 2j,m)J^{(1)}(n,n',l,l\pm 2j,a),$$

where:

$$D^{(k)}(n,n',l,l',a) = \int_0^\infty dr R_{n'l'}(a,r)r^k\frac{\partial}{\partial r}R_{nl}(a,r)$$

The integrals for $D^{(k)}$ and $J^{(k)}$ were evaluated analytically and the integral for $I(l,l',m)$ was evaluated numerically. The matrix, H_0, was diagonalised and the ground state energy converged using a basis of 91 deformed hydrogenic orbitals. We minimised the ground state energy, E, by varying the Bohr radius a and adjustable parameter β to give a ground state energy of -31.23meV, and $a=23.81\dot{A}$, $\beta=0.63$ a.u. and $b=\sqrt{(\gamma/\beta)}a=13.68\dot{A}$ (c.f. Kohn's results of $a=25\dot{A}$ and $b=14.2\dot{A}$ [11], [12]). Table 1 gives a summary of our results in comparison with Faulkner's results and the experimental energies.

Experimentally the ground state splits up into a singlet with A_1 symmetry, a triplet with T_2 symmetry and a doublet with E symmetry. Table 1 shows that Faulkner's method is able to predict the higher donor excited states very well.

The ground state wave function is plotted in figure 1, to show the anisotropy in the z direction, plotted also in figure 1 is the isotropic $1s$ hydrogen orbital for comparison with the deformed hydrogenic orbitals used in basis.

5 Including the Electric Field and Interface Potentials

To accommodate the effect of the applied field and the boundaries on the donor electron wave function it is necessary to use more than one simple bulk ground state wave function to characterise the envelope function. The method we used is favourable because we expand the envelope wave function in a basis of deformed

Table 1: Zero field energies and states for P donor electron.

E(meV)	State	Faulkner's results	Experimental Results
-31.23	$1S$	-31.27	A_1 -45.5
			T_2 -33.9
			E -32.6
-11.12	$2P_0$	-11.51	-11.46
-8.28	$2S$	-8.83	
-6.35	$2P_\pm$	-6.40	-6.40
-5.06	$3P_0$	-5.48	-5.47
-4.46	$3D_0$	-4.75	
-3.62	$3S$	-3.75	

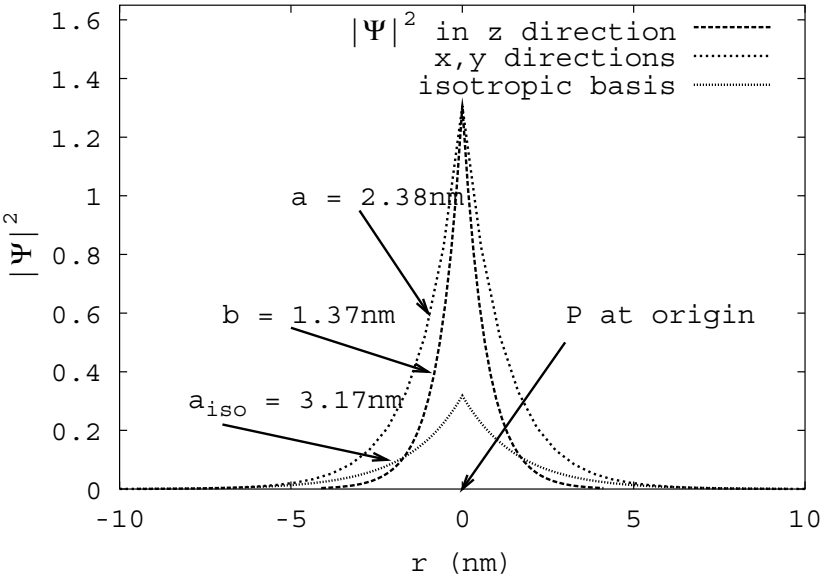

Figure 1: Ground state electron density without electric field.

hydrogenic orbitals which have the flexibility to distort with the applied fields.

Faulkner's method was extended to include the effects of an electric field above the qubit, and boundary conditions of the silicon host. The solution of Poisson's equation to extract the electric field potential for our device with the A and J-gates at varying voltages was obtained by simulation using a Technology Computer Aided Design (TCAD) modelling package.[28] We also added an additional potential to model the SiO_2 layer and back gate interfaces.

TCAD is used in the electronics industry as a tool for 2-D and 3-D modelling and simulation of semiconductor devices. It employs a coupled Newton-like solver at discrete nodes to obtain the self-consistent solution of the Poisson and electron-hole continuity equations. Figure 2 shows the 2-D device scheme implemented in TCAD to model the application of a voltage to either an A or J-gate above qubit, Q_1. The lateral edges of the silicon lattice were assumed to extend infinitely in the y-direction, but the electrostatic potential was only obtained on a finite grid 210nm wide, with the potential set to zero outside this region. We checked that this approximation is valid at the boundaries and found the TCAD potential had fallen close to zero ($10^{-4} - 10^{-5}$eV), at $y = \pm 105$nm, for a voltage of 1.0V at the A-gate. The potential in 2-D from TCAD is assumed to have a "thickness" in the third dimension (x) of 1μm, and the metallic gates were modelled as thin wires in the x direction.

The application of a potential, and the silicon host geometry in the device shown in figure 2 splits the degeneracy of the six conduction band minima, as the electric field potential is not the same in any of the x, y or z directions. We can formulate the problem using a co-ordinate system with the z-axis in the direction from Q_1 to the interface. Using this convention we expand the donor wave function around the conduction band minimum oriented along the z-axis. Because of the smaller effective Bohr radius in the z direction towards the interface and back gate, the ground state is lower in energy since there is less penetration of the wave function into these barrier regions.

We fix the zero field effective Bohr radii in our basis functions, and add an additional matrix, H_1, which contains the electric field and interface potential terms. With the electric field the Hamiltonian is: $H = H_0 + H_1$, where H_0 is the zero field Hamiltonian, and $H_1 = V_{elec}(y, z) + V_i(z)$ is the electric field and interface potential terms. Here $V_{elec}(y, z)$ is the electric field potential generated from TCAD, and we add an additional term, $V_i(z)$, to model the SiO_2 layer and the back gate. The Si/SiO_2 barrier was modelled as a step function with height 3.25eV, since most insulators have a work function greater than 3eV.[29] The back gate serves as a reference voltage point (ground) to the voltages applied to the top gates. Outside the back gate the potential was set at 3.25eV also.

To calculate the perturbed donor electron wave function and energies we constructed the electric field Hamiltonian matrix, H_1, with its elements given by:

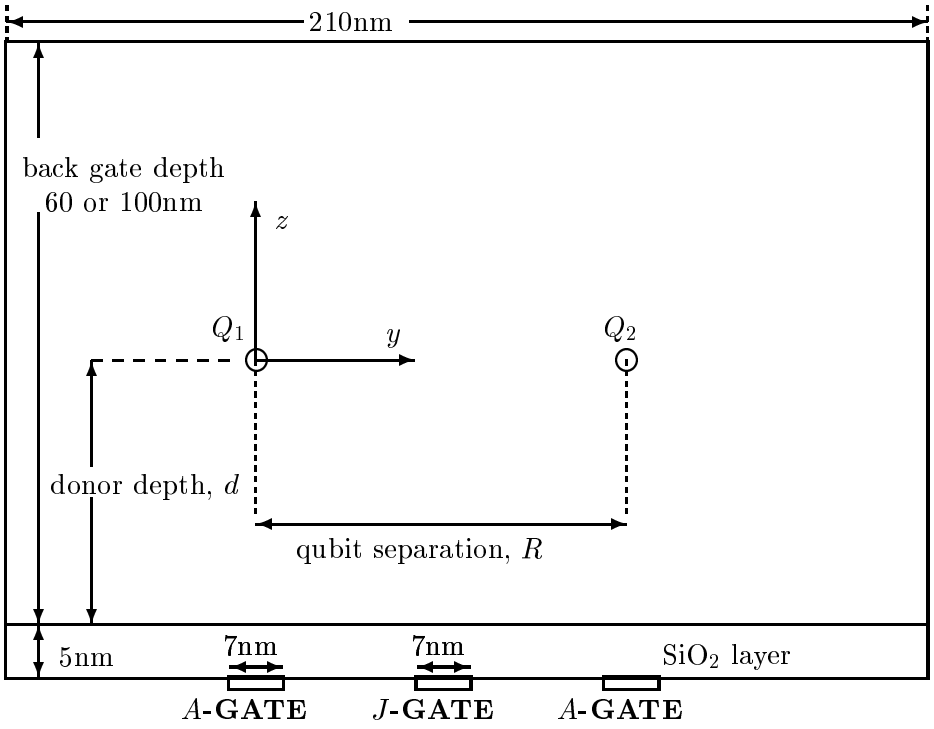

Figure 2: Schematic design parameters implemented in TCAD to model the Kane computer architecture.

$$\langle n'l'm'|H_1|nlm\rangle = \sqrt{\frac{\beta}{\gamma}}\int dx^3 \psi^*_{n'l'm'}(x,y,\sqrt{\frac{\beta}{\gamma}}z,a)\Big[V_{elec}(y,z)+V_i(z)\Big]\psi_{nlm}(x,y,\sqrt{\frac{\beta}{\gamma}}z,a). \quad (12)$$

The integrals in equation (12) were calculated numerically for the varying gate voltages and qubit position. Once H_1 was obtained the total Hamiltonian was then diagonalised to find the donor electron ground state with the varying experimental parameters.

6 Calculation of the hyperfine interaction coupling and exchange splitting

For the Si:P quantum computer to be feasible, quantum operations have to be able to be applied selectively to particular nuclear spins, and connectivity between nuclear

spins via electron-mediated coupling must be established. To achieve both these goals it is necessary to study the degree of selectivity and connectivity that can be controlled by applying electric fields to metal gates above (A-gates) and adjacent (J-gates) to spins. Furthermore, it is shown in this paper that the qubit location in the device in relation to each other (inter donor separation) and to the gates (donor depth below the silicon oxide barrier), also has a significant influence on the donor electron wave function.

Once the perturbed donor electron ground state was obtained we calculated the hyperfine and exchange coupling as a function of the varying experimental conditions. We did this in order to compare and optimise the conditions necessary for addressing the target qubits, Q_1 and Q_2.

6.1 Calculation of the contact hyperfine interaction

The general formula for the contact hyperfine coupling $A(V)$ with an applied voltage, V, at the gate, is given below:

$$A(V) \quad = \quad \frac{2}{3}\mu_B g_N \mu_N \mu_0 |\Psi(V,\mathbf{0})|^2,$$

where $\Psi(V,\mathbf{0})$ is the donor electron ground state wave function evaluated at the donor nucleus, μ_B is the Bohr magneton, g_N is Lande's factor for ^{31}P, μ_N is the nuclear magneton and μ_0 is the permeability of free space.[19, 20]

Since we use effective mass theory, instead of calculating the donor wave function with the full expansion of the Bloch functions, we calculate the envelope function, which describes the smooth donor-related modulation of the electron wave-function. So instead of calculating the contact hyperfine coupling, $A(V)$, directly we calculate the relative shift in $A(V)$ with the potential applied and assume this shift will be similar to those of the true wave function.[20] Thus we need to calculate:

$$A(V) \quad = \quad \frac{|\Psi(V,\mathbf{0})|^2}{|\Psi(0,\mathbf{0})|^2} A(0), \tag{13}$$

where $A(0)/h = 28.76$MHz is determined for ^{31}P in silicon from experimental data,[19, 1] and $\Psi(V,\mathbf{r})$ are the donor envelope wave functions calculated by our method.

6.2 Calculation of the exchange splitting for an impurity pair

In this section we employ a Heitler-London (H-L) treatment of the two electron donor pair wave function, using the two single donor ground state wave functions perturbed by the electric field as our basis. Since the donor ions are generally well separated in the silicon wafer device we can justify using H-L theory to describe the two electron system as the symmetrised and anti-symmetrised products of the single donor orbitals at each qubit ($\Psi^{Q_1}(V,\mathbf{r})$ and $\Psi^{Q_2}(V,\mathbf{r})$) calculated with the electric

field applied. The singlet and triplet impurity donor pair wave functions are given by:[31]

$$\Psi(V,\mathbf{r}) = \Psi^{orbit}_{\substack{S\\T}}(V,\mathbf{r})\chi^{spin}_{\substack{S\\T}},$$

where:

$$\begin{aligned}\Psi^{orbit}_{\substack{S\\T}}(V,\mathbf{r}) &= \frac{1}{\sqrt{2(1\pm S^2)}}\Big[\Psi^{Q_1}(V,\mathbf{r_1})\Psi^{Q_2}(V,\mathbf{r_2}-\mathbf{R}) \pm \Psi^{Q_1}(V,\mathbf{r_2})\Psi^{Q_2}(V,\mathbf{r_1}-\mathbf{R})\Big],\\ S &= \int \Psi^{Q_1}(V,\mathbf{r})\Psi^{*Q_2}(V,\mathbf{r}-\mathbf{R})dr^3.\end{aligned}$$

Here $\Psi^{Q_1}(V,\mathbf{r})$ and $\Psi^{Q_2}(V,\mathbf{r}-\mathbf{R})$ are the single wave functions calculated using our basis of deformed hydrogenic orbitals, and diagonalising the Hamiltonian for the varying voltages at the J-gate and qubit position. We are using the the co-ordinate system shown in figure 3 for our two-electron system.

We observe that $\Psi^{Q_2}(V,x,y,z) = \Psi^{Q_1}(V,x,-y+R,z)$, as the donor wave functions on adjacent nuclei have reflection symmetry about the y-axis when a voltage is applied to the J-gate (see figure 2).

To calculate the exchange splitting between the ground singlet and triplet states for an impurity pair of donors in silicon we use the H-L formula:[31]

$$\begin{aligned}J(R) &= E_T - E_S\\ &= \langle\Psi_T|H_{2e}|\Psi_T\rangle - \langle\Psi_S|H_{2e}|\Psi_S\rangle\\ &= \frac{2}{1-S^4}\left(S^2K_0 - K_1\right), \qquad (14)\end{aligned}$$

where:

$$\begin{aligned}H_{2e} &= -\nabla^2_{anis}(\mathbf{r_1}) - \nabla^2_{anis}(\mathbf{r_2}) - \frac{2}{|\mathbf{r_1}|} - \frac{2}{|\mathbf{r_2}|} - \frac{2}{|\mathbf{r_1}-\mathbf{R}|} - \frac{2}{|\mathbf{r_2}-\mathbf{R}|}\\ &+ \frac{2}{|\mathbf{r_1}-\mathbf{r_2}|} + V_{elec}(\mathbf{r_1}) + V_{elec}(\mathbf{r_2}) + V_i(\mathbf{r_1}) + V_i(\mathbf{r_2}),\\ K_0 &= \int |\Psi^{Q_1}(V,\mathbf{r_1})|^2|\Psi^{Q_2}(V,\mathbf{r_2}-\mathbf{R})|^2\Theta dr_1^3 dr_2^3,\end{aligned}$$

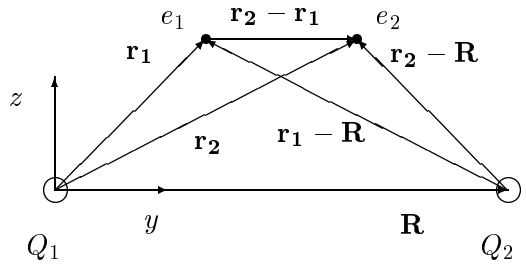

Figure 3: Co-ordinate geometry of our two-electron problem.

$$K_1 = \int \Psi^{*Q_1}(V, \mathbf{r_2})\Psi^{*Q_2}(V, \mathbf{r_1} - \mathbf{R})\Psi^{Q_1}(V, \mathbf{r_1})\Psi^{Q_2}(V, \mathbf{r_2} - \mathbf{R})\Theta dr_1^3 dr_2^3,$$

$$\Theta = \frac{2}{|\mathbf{r_2} - \mathbf{r_1}|} - \frac{2}{|\mathbf{r_1} - \mathbf{R}|} - \frac{2}{|\mathbf{r_2}|}.$$

Once the perturbed ground state under the applied field was obtained we calculated the contact hyperfine interaction and the exchange splitting (using equations (13) and (14) respectively), for the impurity donor pair, to optimise and determine the experimental conditions needed to control the nuclear spins coupling to the donor electron spin, via the hyperfine interaction, and to other nuclei via the electron-mediated exchange interaction.

So far we have only considered the effect of the A or J-gate independently. The smaller inter donor distances ($R \leq 14$nm) are only possible if the gate dimensions can be reduced to prevent overlapping gates. In this initial study, we aim to give insight into, and identify the relevant factors that contribute to the hyperfine and exchange coupling, which need to be studied more in depth.

7 Results with the A-gate voltage applied

7.1 Results obtained varying A-gate voltage and donor depth

In this section, we varied the voltage at the A-gate directly above the qubit and the qubit depth below the SiO_2 layer. The proximity of the qubit to the gate plays a vital role in determining the extent to which the gate voltage affects the donor electron. We find that depending on the distance of the donor to the gate, and the magnitude of the gate potential, the electron transfer to the gate is either gradual or abrupt. The calculations in this section were all performed using a back gate depth at 60nm.

For shallow donor depths the electron is only slightly perturbed by the positive gate voltage, as the P nucleus and the gate are so strongly "coupled"[21] that the effect of the gate voltage is only to further bind the donor electron to both the nucleus and the gate. In contrast, at larger donor depths the electron is perturbed or ionised almost completely away from the nucleus to the gate, for large enough positive voltages. The location of the silicon oxide interface also restricts the donor electron wave function at shallow donor depths from perturbing towards the positive gate potential.

This phenomena is reflected in figures 4(a) and (b), where we observe the difference in the donor electron ground state obtained for a donor depth of 20 and 40nm with a positive voltage of 1.0V at the A-gate. In both these plots the donor wave function moves toward the applied A-gate voltage in the negative z direction. For a close donor depth of 20nm we observe that even though the donor wave function moves slightly toward the A-gate, it is significantly restricted in moving in this direction because of the silicon oxide interface in this direction also. In contrast the

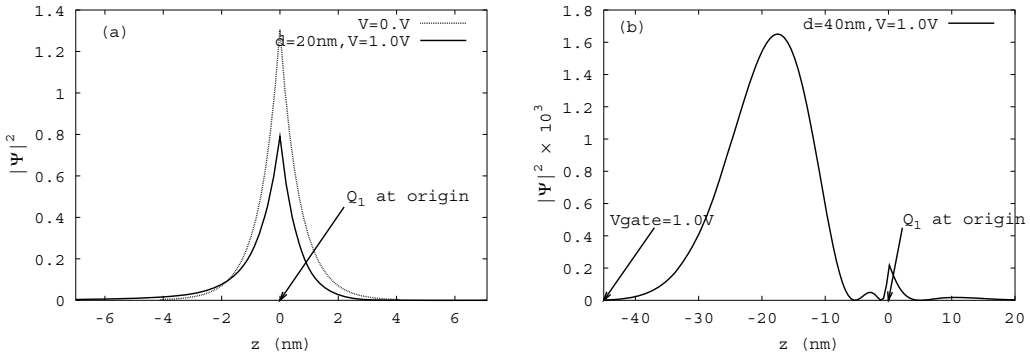

Figure 4: Ground state electron density in z-direction, for a donor depth of 20nm in (a) and 40nm in (b), with a voltage of 1.0V at the A-gate. Note the different vertical scales of $|\Psi|^2$ in (a) and (b).

donor wave function for a depth of 40nm deforms unhindered toward the A-gate, and most of the electron density has been transformed away from the nucleus.

Figure 5 shows the donor electron density obtained in the yz-plane for a negative voltage of -1.0V at the A-gate and a donor depth of 20nm. A negative applied voltage causes the electron to disperse in all directions away from the positive potential, this plot demonstrates that because of the close back gate in the positive z-direction, the electron density predominantly perturbs away from the applied voltage in either direction laterally.

Figure 6 shows the magnitude of the contact hyperfine interaction calculated for the varying donor depths and A-gate voltage. As the donor electron density decreases at the nucleus, so does the contact hyperfine interaction. For the lower voltages ($\leq$ 0.8V) in figure 6, the results are consistent with the expectation that the closer the donor depths are to the applied voltage, the greater the donor electron wave function is perturbed by the applied voltage. But at voltages above a certain threshold and donor depths further away from the silicon oxide barrier, there is a huge difference in the donor wave function from the zero field ground state, as it is perturbed almost completely away from the nucleus.

When the electron is perturbed or ionised completely away from the nucleus, the contact hyperfine interaction decreases almost to zero. Because of the interface regions it is either energetically favourable for the donor electron wave function at shallow donor depths to distort completely away from the nucleus, when the gate voltage is negative, or for the donor wave function to be restricted in distorting towards the A-gate, with a positive voltage.

This contrast in the donor electron wave function at different donor depths occurs because as the qubit moves further from the gate, the electron has to overcome a "barrier" to distort towards the gate. At large enough positive voltages the potential well at the A-gate is deep enough to trap the electron at the A-gate. The

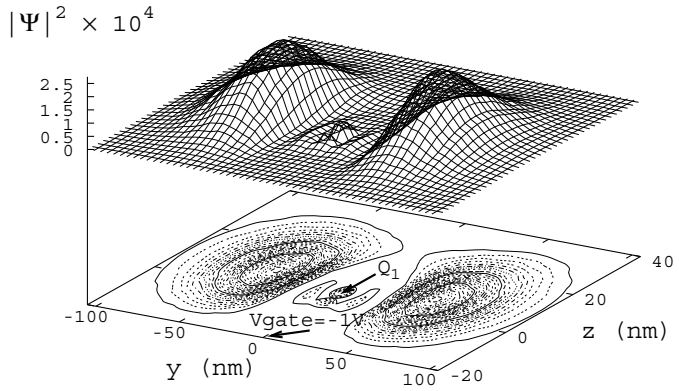

Figure 5: Ground state electron density in the yz-plane for donor depth at 20nm and voltage at -1.0V at the A-gate, in the yz-plane. We have also included the location of the qubit at the origin and the A-gate in the contour plot.

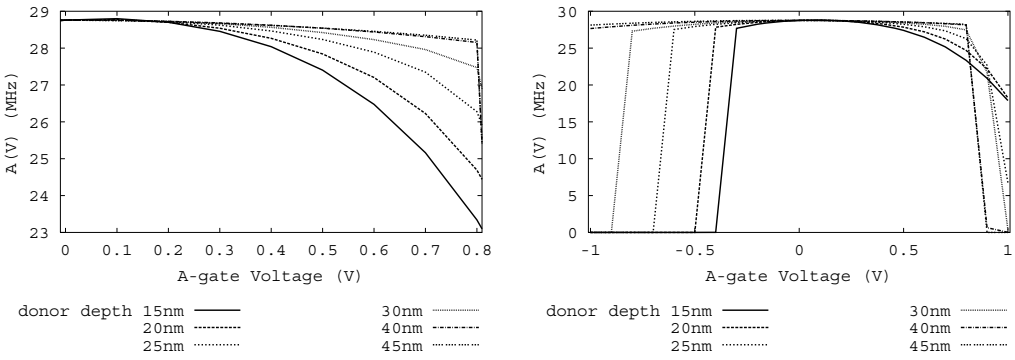

Figure 6: Contact hyperfine interaction at varying voltages and donor depth.

basis we are using for the donor electron consists only of bound states, which is a good approximation for the smaller voltages when the electron is still bound to the nucleus. To model the ionisation process at larger gate voltages more accurately, a more rigorous approach would be to include the delocalised conduction band states in the basis as well.

In Table 2 we present a comparison of the difference in the ground state energy for the donor wave function without the electric field (E_0), and with a positive voltage of 1.0V applied to the A-gate (E_{1V}), for two different donor depths. Also reported in this table is the TCAD potential at the P nucleus for the varying donor depths. For the close donor depth at 20nm we observe that the energy difference is approximately equal in magnitude to the TCAD potential at the nucleus. This is because the donor wave function has perturbed only slightly from the zero field ground state wave function. In contrast the energy difference for the donor depth at 40nm is much higher as the wave function deforms significantly from the ground state wave function towards the applied voltage.

Table 2: $E_{1V} - E_0$ for a back gate depth of 60nm.

Q_1 Depth (nm)	TCAD Potential at Q_1 (meV)	$E_{1V} - E_0$ (meV)
20	-90.02	-91.70
40	-37.06	-47.73

7.2 Results obtained varying back gate depth and donor depth

To observe the effect that the back gate depth has on the donor electron wave function we repeated the calculations for a voltage of 1.0V at the A-gate, with a back gate depth at 100nm. Figure 7 shows the comparison between contact hyperfine interaction calculated for a voltage at the A-gate with a close and far back gate. These calculations were performed with a close back gate at 60nm and a far back gate at 100nm, with a bias of 1.0V at the A-gate and donor depths ranging from 30 to 75nm.

With a closer back gate the electric field strength is higher within the Si wafer. Because of this the donor electron wave function is perturbed greater by the applied voltage with a closer back gate. Thus the contact hyperfine interaction is close to zero for a back gate at 60nm and the donor depths studied in this section ($30 \leq d \leq 45$nm). With the back gate at 100nm, the electric field strength is lower, and there is no substantial overlap of the donor electron wave function with the back gate barrier for donor depths of 30 and 40nm, so it is not as energetically favourable for the donor electron to perturb away from the back gate toward the A-gate.

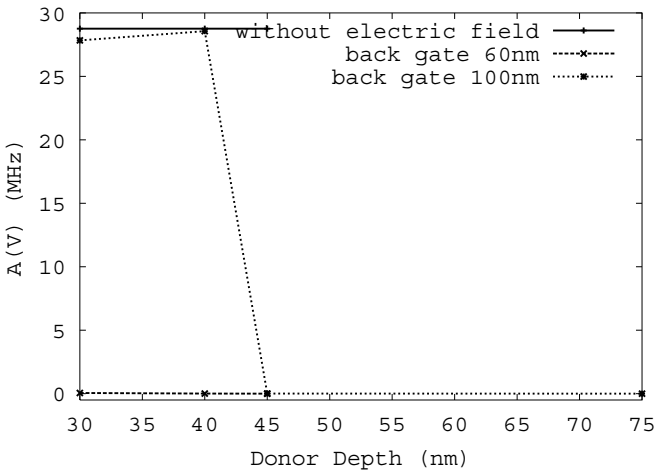

Figure 7: Contact hyperfine interaction at varying donor depths with back gate depth at 60 and 100nm, and 1.0V at A-gate.

Table 3: $E_{1V} - E_0$ for a back gate depth of 100nm.

Q_1 Depth (nm)	TCAD Potential at Q_1 (meV)	$E_{1V} - E_0$ (meV)
40	-67.25	-68.33
75	-26.00	-36.57

Figure 8 shows the ground state electron density plotted in the yz-plane for a donor depth of 75nm, and a back gate depth of 100nm, and a positive voltage of 1.0V at the A-gate. This plot demonstrates that even at a donor depth far from the A-gate, the ground state wave function distorts freely toward the A-gate because of the close proximity of the back gate, and the remoteness of the silicon oxide interface.

In Table 3 we present a comparison of the difference in the ground state energy for the donor wave function perturbed by a voltage of 1.0V applied to the A-gate and a back gate at 100nm, for two different donor depths, $d = 40$ and 75nm. Also reported in this table is the TCAD potential at the P nucleus for the varying donor depths. This table reflects the trend noted in Table 2 that a significantly lower ground state energy is obtained for the deeper donor depths, where the electron density perturbs significantly away from the nucleus toward the applied voltage.

7.3 Conclusions with the A-gate voltage applied

We compared our results which included the effects of both the interface regions and electric field potentials, to Kane's[18] results wherein only the potential of a

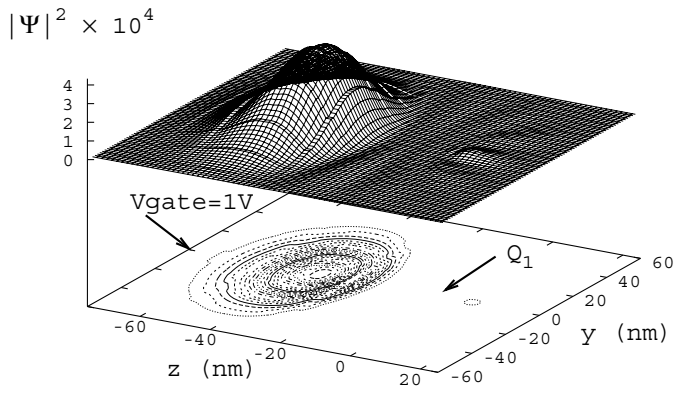

Figure 8: Ground state electron density in yz-plane for donor depth at 75nm with back gate depth of 100nm, and 1.0V at A-gate. We have also included the location of the qubit at the origin and the A-gate in the contour plot.

uniform electric field in the bulk was considered. We found that the SiO_2 layer and the back gate exert a substantial influence on the donor electron wave function. Instead of the contact hyperfine coupling, $A(V)$, being independent of whether a positive or negative voltage is being applied at the A-gate as reported by Kane, we found that the effect of whether a positive or negative voltage is applied at the A-gate causes very different changes in the donor electron density. For a positive voltage the electron is bound to both the nucleus and the A-gate. In contrast, when a high enough negative voltage is applied so that the electron is no longer bound to the P nucleus, the electric field profile causes the electron to disperse in all directions away from the positive potential.

The donor wave function exhibits a fundamental change at crucial experimental parameters, where the electron wave function transforms from being only slightly perturbed from the zero field ground state, to being almost completely perturbed away from the nucleus. These results highlight the significance of the influence of the silicon host geometry on the donor electron wave function.

8 Results with the J-gate voltage applied

We performed similar calculations as the previous section, but instead we consider a voltage applied to the J-gate. This means we have an additional experimental variable which can be tuned, the inter donor separation. The function of the J-gate is to draw the electrons on adjacent qubits closer together, to enhance the

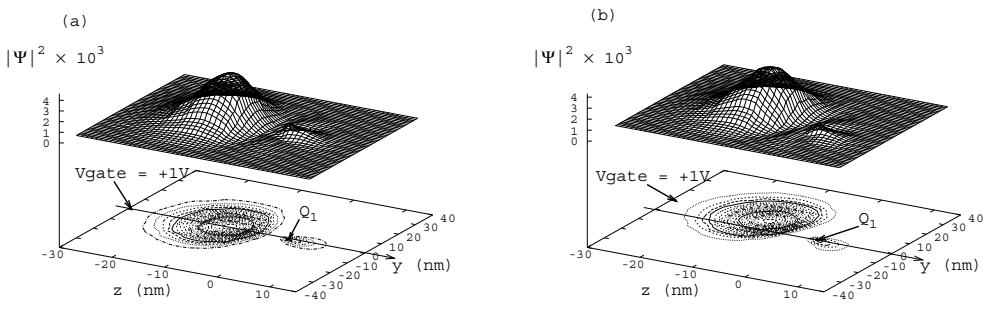

Figure 9: Ground state electron density in yz-plane for donor depth at 30nm with 1.0V at the A-gate in (a) and J-gate with $R = 20$nm for (b). In both plots Q_1 is located at the origin, and we have included the $y = 0$ symmetry line in the contour plot, to highlight the difference in the electron density for an applied A or J-gate voltage.

exchange interaction between them. In addition to calculating the variance of the hyperfine coupling with the applied voltage and qubit position, we also calculated the exchange coupling as a function of the experimental parameters: gate voltage, donor depth, and inter donor separation.

The symmetry along the $y = 0$ line is destroyed when a J-gate voltage is applied. Figures 9(a) and (b) shows the comparison between the electron ground state probability density in the yz-plane, obtained for a voltage of 1.0V applied to the A and J-gate respectively, for a donor depth of 30nm and inter donor separation of R =20nm. For an A-gate voltage, the donor wave function is symmetric in y and only perturbs toward the A-gate in the z direction. In comparison, when a J-gate voltage is applied, the wave function can distort in both the y and z directions. Unfortunately as the donor depth becomes greater, selectivity may be lost, and a voltage applied at either the A or J-gate will cause the same change in the contact hyperfine interaction.

Similarly with a negative voltage applied at the J-gate, the donor electron ground state is deformed away from the applied voltage in the negative y-direction only. This difference is demonstrated again in figure 10.

8.1 Results obtained varying gate voltage and inter donor separation

8.1.1 Results for the contact hyperfine interaction

To demonstrate the effect of J-gate voltage and inter donor separation on the donor electron ground state, we calculated the perturbed single electron donor ground

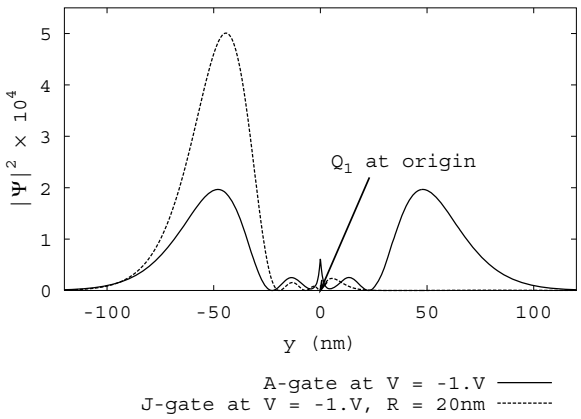

Figure 10: Ground state electron density in y-direction for a donor depth at 20nm with -1.0V at the A-gate and J-gate, with $R = 20$nm. Q_1 is located at the origin.

states as a function of these external factors. The calculations in this section were obtained at a donor depth of 20nm.

Figure 11 shows the magnitude of the contact hyperfine interaction calculated for varying qubit separation and gate voltage. These results reflect the trend that as the qubit moves away from the J-gate, the donor electron wave function has more freedom to move towards the J-gate and distort greater.

Figure 12 demonstrates this behaviour, it shows an example of the donor ground state wave functions of Q_1 and Q_2 for an applied voltage of 1.0 V at the J-gate, for two inter donor separations, $R = 14$ and 20nm. We can observe from the relative magnitudes of the ground state electron densities of the two qubits that the ground state wave functions for the larger inter donor separation, $R = 20$nm, have perturbed more towards the J-gate voltage.

For certain negative gate voltages the contact hyperfine interaction $A(V) \approx 0$, which indicates that the donor wave function has distorted completely away from the nucleus. For $R \leq 14$nm, and $V \leq -0.5$V, the qubit is no longer bound to the nucleus, and disperses completely away from the applied voltage. Similarly for $16 \leq R \leq 20$nm, and $V \leq -0.6$V, the qubit is no longer bound to the nucleus.

This is illustrated in figure 13 where we see an abrupt change in the donor wave functions going from $R = 14$ to 16nm for a voltage of -0.5 V at the J-gate. Here the electron density for $R = 14$nm is 100 times smaller than that for $R = 16$nm. For R=14nm the electron is no longer bound to the nucleus and has dispersed from the negative applied voltage in all directions. In contrast the wave function for $R = 16$nm is still bound to the nucleus and only perturbed slightly by the applied negative voltage.

The effect of the gate voltage on the donor electron depends on the distance of

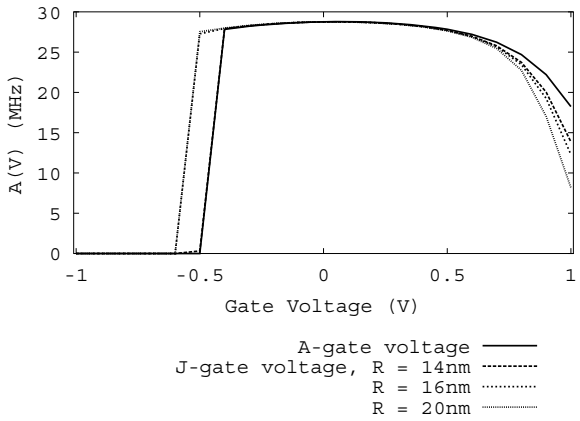

Figure 11: Contact hyperfine interaction at varying gate voltage and inter donor separation, for a donor depth of 20nm.

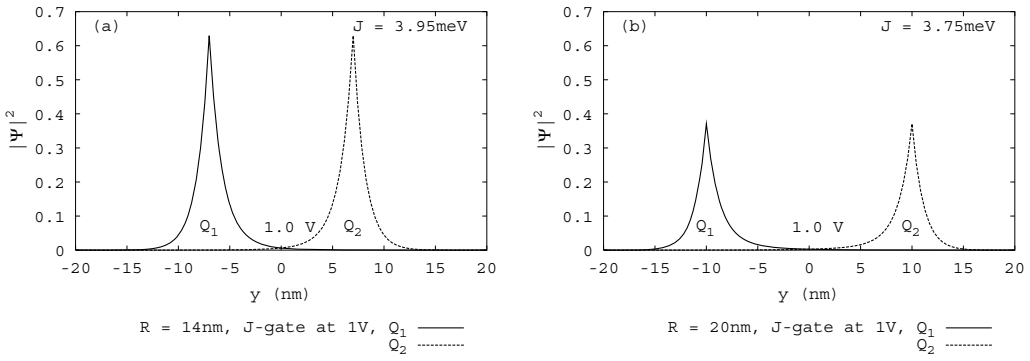

Figure 12: Ground state electron densities of Q_1 and Q_2, in y-direction at $z = 0, x = 0$ for an inter donor separation of $R = 10$ and 20nm, a donor depth of $d = 20$nm and a voltage of 1.0 V at the J-gate.

the qubit from the gate.[9, 23, 21] At the experimental parameters considered in this section ($d = 20$nm and $R \leq 20$nm), the qubits are situated at relatively short distances from the J-gate. So for positive voltages the electron transfer to the gate with increasing J-gate voltage is gradual.[21] However for negative J-gate voltages, there is an abrupt change in the electron density at the nucleus for critical negative voltages where the electron is no longer bound to the nucleus.

8.1.2 Results for the exchange splitting

We evaluated the zero field exchange interaction in bulk Si for varying inter donor separation, in order to compare our results with published work. We found that

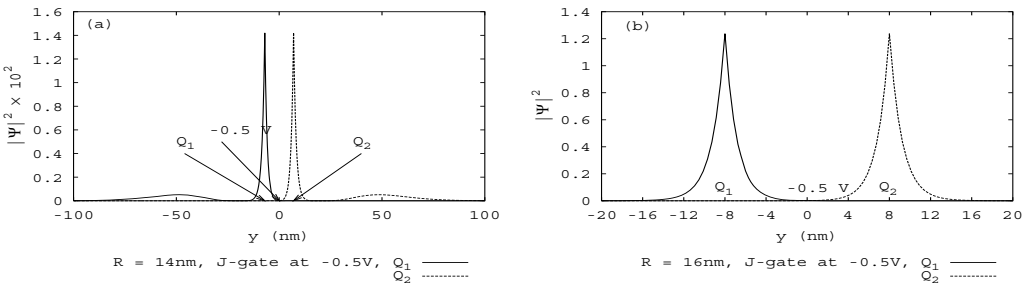

Figure 13: Ground state electron densities of Q_1 and Q_2, in y-direction at $z = 0, x = 0$ for an inter donor separation of $R = 14$ and 16nm, a donor depth of $d = 20$nm and a voltage of -0.5 V at the J-gate. Note the different vertical scales of $|\Psi|^2$ in (a) and (b).

our results using the larger effective Bohr radius, along the inter donor axis, and the smaller effective Bohr radius, toward the SiO_2 layer, gave results which are consistently higher than other reported theoretical values using H-L theory.[14, 15, 13, 23] This is because we chose the larger effective Bohr radius, $a = 2.381$nm, to be along the inter donor axis, and hence the exchange splitting is larger using this convention. The larger effective Bohr radius was chosen to be along the inter donor axis so that it would also be towards the positive J-gate potential, and the smaller Bohr radius in the direction towards the interfaces.

In this paper we are trying to model the effects of the electric field potential and Si host geometry on the donor wave function, to investigate the variation of the exchange splitting with the applied voltage, rather than the absolute values of $J(R)$. Koiller *et al.*[14] calculated the exchange coupling in uniaxially strained Si in the presence of interfaces, and also found that these environmental influences could affect the exchange coupling significantly. They found that the $F_{\pm}(z)$ envelopes were favoured energetically, because the smaller effective Bohr radius in the z-direction guarantees less significant penetration of the wave function into the barrier regions.

Figure 14 shows the exchange coupling as a function of inter donor separation and positive J-gate voltage. The exchange coupling increases as the J-gate voltage increases as expected, since the applied field draws the electrons closer together. At a voltage of 1.0V the donor electron wave function is perturbed the greatest, and the exchange coupling is significantly higher at this voltage for every inter donor separation.

We expect the exchange coupling to decrease with increasing inter donor separation, and this is the case for voltages less than 1.0V. However in figure 14(b), we observe that for for a voltage of 1.0V and for $R = 20$nm, the exchange coupling actually increases slightly. This is because at large inter donor separations the donor is further from the J-gate, and thus is more attracted to the potential well at the

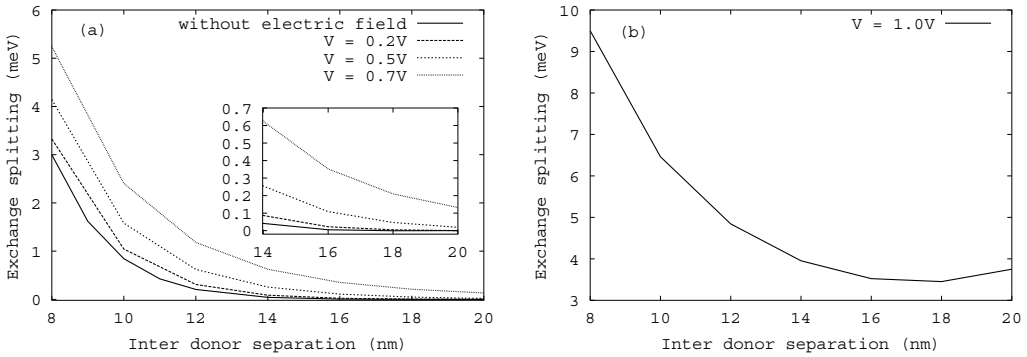

Figure 14: Calculated exchange coupling as a function of inter donor distance and positive J-gate voltage, (a) is the results for $V \leq 0.7$V and (b) for $V = 1.0$V, for a donor depth of 20nm.

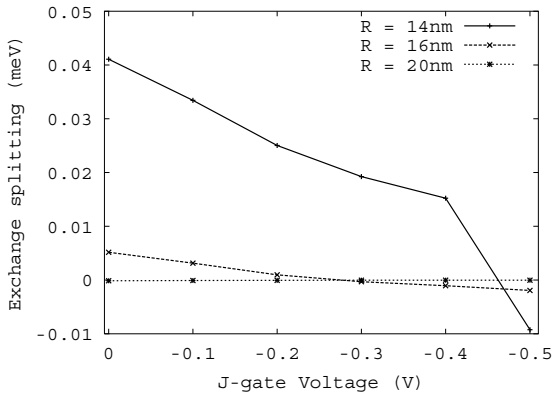

Figure 15: Calculated exchange coupling as a function of inter donor distance and negative J-gate voltage, for a donor depth of 20nm.

J-gate as the gate voltage increases sufficiently. Hence the overlap between the adjacent donor electron orbitals is slightly greater, even if the inter donor separation is higher.

Figure 15 shows that if we apply a large enough negative voltage to the J-gate, we can effectively turn off the coupling between the two qubits. As predicted the exchange coupling decreases as the negative applied potential also decreases. When the applied negative voltage is large enough, the electron densities at Q_1 and Q_2 are greatly perturbed from J-gate in opposite directions, and we have effectively turned off the coupling between the adjacent qubits, as the overlap between the two electron densities is almost zero. This has been demonstrated already in figure 13(a) that for a voltage of -0.5V at the J-gate and R =14nm, the donor wave functions

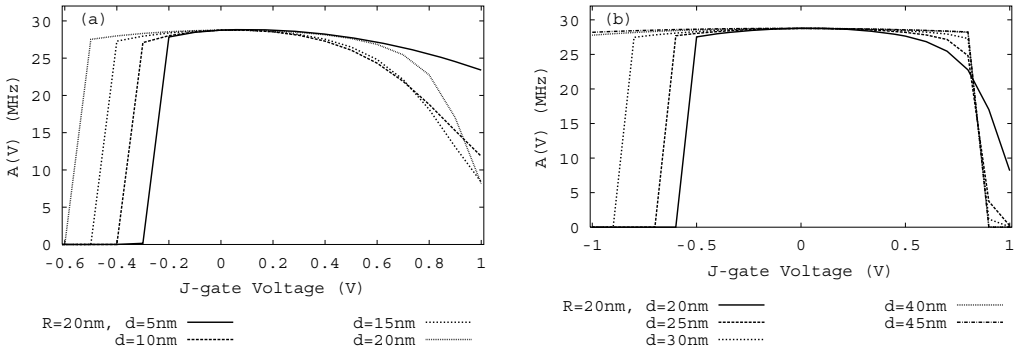

Figure 16: Contact hyperfine interaction at varying donor depths and J-gate voltage, with inter donor separation $R = 20$nm.

for Q_1 and Q_2 have perturbed away from the applied voltage in opposite directions.

8.2 Results obtained varying the gate voltage and donor depth

We observed the effect that the donor depth, d, below the silicon oxide layer has on the donor ground state perturbed by a gate voltage. Here we ran calculations for $5 \leq d \leq 45$nm.

8.2.1 Results for the contact hyperfine interaction

Figure 16 show our results for the contact hyperfine interaction at varying donor depth and gate voltage. We observe similar trends in the variation of the hyperfine interaction with a J-gate bias, as in the previous section with an A-gate bias. As d increases, (and hence the distance from the J-gate also increases), we see a cross-over behaviour where the donor wave function is perturbed greater for larger donor depths at positive voltages above a critical value. In figure 16(b) for $d \geq 25$nm, there is an abrupt decrease in the electron density for $V \geq 0.9$V, defining an ionisation voltage at these donor depths. This process of ionisation has been reported previously.[9, 10, 21]

8.2.2 Results for the exchange splitting

Figure 17 shows the variation of the exchange coupling with donor depth and voltage for two inter donor separations, $R = 14$ and 20nm. It is evident that the depth of the donor influences the degree to which the electron is perturbed by the gate voltage, and hence will also affect the strength of the exchange coupling.

For small d, the electron is less affected by the positive gate voltage, as the P nucleus and the gate voltage are so physically close together that the two wells can

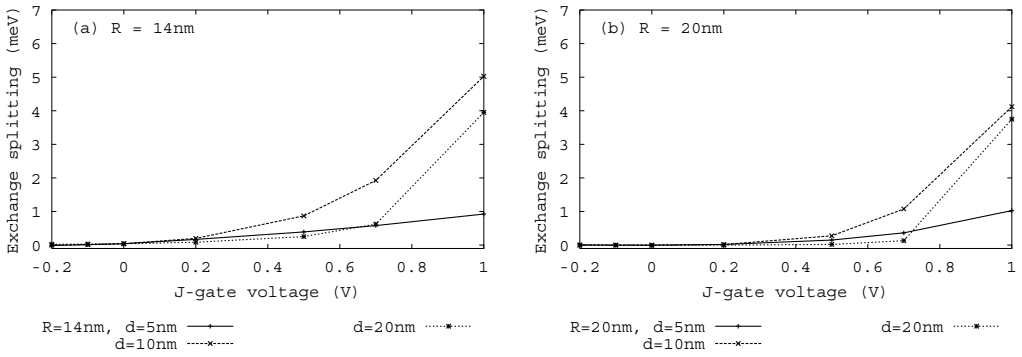

Figure 17: Calculated exchange coupling as a function of donor depth and J-gate voltage, with R=14nm in (a), and R=20nm in (b).

be considered as a single well, the position of which is pulled towards the gate with increasing gate voltage. [21] So we see for $d = 5$nm that although the exchange coupling has increased significantly from the zero field coupling, it is still not as strong as the coupling for $d = 10$ and 20nm.

The exchange coupling for $d = 10$ and 20nm are similar, and the effect of the magnitude of d is not so pronounced. We observe that at a donor depth of 10nm the exchange coupling is enhanced the most by the applied voltage. One of the reasons for this may be that for $d = 10$nm, the donor wave functions predominantly move toward the applied voltage at the J-gate in the y-direction along the inter donor axis and thus the exchange coupling is enhanced further. Whereas for a deeper donor depth at $d = 20$nm, the wave functions can perturb in both the y and z-directions toward the J-gate.

We did not obtain the exchange coupling for donor depths > 20nm because at donor depths further away from the silicon oxide layer, the donor electron wave function for Q_1 and Q_2 can deform unhindered toward the J-gate for $V \geq 0.9$V. At these depths and large enough voltages, the electron wave function transforms almost completely away from the donor nucleus. Because of this the electron wave functions at Q_1 and Q_2 no longer resemble a close approximation to two separate wave functions at each nucleus, and H-L theory is no longer a valid approximation. Future developments in our laboratory are concentrating on deriving a more rigorous evaluation of the donor exchange coupling, which extends the H-L basis.

8.3 Conclusions with the J-gate voltage applied

The results presented highlight the significance of not only the gate potential in addressing the qubit, but also the position of the donors in the device. In the absence of an electric field, only the inter donor separation is instrumental in determining the strength of the exchange coupling, and as R increases the exchange coupling

decreases. However, when a large positive voltage is applied at the J-gate, either a gradual transference of the donor electron density occurs for dopants close to the gate, and the exchange coupling is enhanced proportionally. Or if the electron is ionised by the gate voltage the exchange coupling can be enhanced considerably even for quite large inter donor separations and donor depths. So both of these competing influences must be considered in modelling the strength of the exchange coupling. We also demonstrated the ability to effectively turn off the exchange coupling with an applied negative voltage at the J-gate.

9 Conclusions and prospects for achieving silicon-based quantum computation

We have studied the P donor wave function perturbed by an electric field and the Si host geometry, and the two interactions fundamental to the Kane quantum computer: the hyperfine and exchange interactions. We have studied the effect of varying several experimental parameters: the gate voltage, inter donor separation, and donor depth in order to fine tune the hyperfine and exchange interaction.

The proximity of the qubit to the gate determines the degree to which the electron can be altered by the applied voltage. It is evident that the P donor electron wave function is sensitive to all experimental parameters studied in this paper. One of the critical discoveries was that the donor electron wave function exhibits a fundamental change at crucial experimental parameters, where the electron wave function transforms from being only slightly perturbed from the zero field ground state, to being almost completely perturbed away from the nucleus. At these experimental parameters the hyperfine interaction and exchange coupling can be changed dramatically from the zero field values.

We believe the results presented here using effective mass theory and calculating the smooth donor-modulated envelope function, provide a solid foundation for future device modelling. We highlight the significance of experimental variables other than the gate potential which have considerable implications for fabrication of these devices. We are currently focusing our efforts to extend these calculations to include the expansion of the donor wave function at all six conduction band minima in the Si crystal, into our approach.

However, including the Bloch wave structure, the inter valley terms and the electric field and interface potentials is a challenging task. The results presented here are quantitatively reasonable and provide a fast and reliable method which gives insight into the behavior of the P donor electron wave function under several different experimental conditions.

Acknowledgments

L.M. Kettle and H.-S. Goan would like to thank C.I. Pakes and G.J. Milburn for valuable discussions relating to this work. This work was supported in part by the Australian Partnership for Advanced Computing National Facility, the Australian Research Council, the Australian Government, the US National Security Agency, the Advanced Research and Development Activity, and the US Army Research Office under contract number DAAD19-01-1-0653. H.-S. Goan would like to acknowledge support from a Hewlett-Packard Fellowship.

References

[1] B.E. Kane, Nature **393**, 133 (1998).

[2] R. Vrijen, E. Yablonovitch, K. Wang, H.W. Jiang, A. Balandin, V. Roychowdhury, T. Mor and D. DiVincenzo, Phys. Rev. A **62**, 012306 (2000).

[3] A.J. Skinner, M.E. Davenport and B.E. Kane, Phys. Rev. Lett. **90**, 087901 (2003).

[4] T.D. Ladd, J.R. Goldman, F. Yamaguchi, Y. Yamamoto, E. Abe and K.M. Itoh, Phys. Rev. Lett. **89**, 017901 (2002).

[5] R. De Sousa, J.D. Delgado and S. Das Sarma, cond-mat/0311403 (2003).

[6] M. Friesen, P. Rugheimer, D.E. Savage, M.G. Lagally, D.W. Van der Weide, R. Joynt and M.A. Eriksson, Phys. Rev. B **67**, 121301 (2003).

[7] L.C.L. Hollenberg, A.S. Dzurak, C.J. Wellard, A.R. Hamilton, D.J. Reilly, G.J. Milburn and R.G. Clark, cond-mat/0306235 (2003).

[8] R.A. Faulkner, Phys. Rev. **184**, 713 (1969).

[9] L.M. Kettle, H.-S. Goan, Sean C. Smith, C.J. Wellard, L.C.L. Hollenberg and C.I. Pakes, Phys. Rev. B **68**, 075317 (2003).

[10] L.M. Kettle, H.-S. Goan, Sean C. Smith, C.J. Wellard and L.C.L. Hollenberg, J. Phys.: Cond. Matter **16**, 1011 (2004).

[11] W. Kohn and J.M. Luttinger, Phys. Rev. **97**, 1721 (1955).

[12] W. Kohn and J.M. Luttinger, Phys. Rev. **98**, 915 (1955).

[13] C.J. Wellard, L.C.L. Hollenberg, F. Parisoli, L.M. Kettle, H.-S. Goan, J.A.L. McIntosh and D.N. Jamieson, Phys. Rev. B **68**, 195209 (2003).

[14] B. Koiller, X. Hu, and S. Das Sarma, Phys. Rev. B **66**, 115201 (2002).

[15] B. Koiller, X. Hu, and S. Das Sarma, Phys. Rev. Lett. **88**, 27903 (2002).

[16] C. Tahan, M. Friesen and R. Joynt, Phys. Rev. B **66**, 35314 (2002).

[17] L.J. Sham and M. Nakayama, Phys. Rev. B **20**, 734 (1979).

[18] B.E. Kane, Fortschr. Phys. **48**, 1023 (2000).

[19] A.A. Larionov, L.E. Fedichkin, A.A. Kokin and K.A. Valiev, Nanotechnology **11**, 392 (2000).

[20] C.J. Wellard, L.C.L. Hollenberg and C.I. Pakes, Nanotechnology **13**, 570 (2002).

[21] G.D.J. Smit, S. Rogge, J. Caro and T.M. Klapwijk, Phys. Rev. B **68**, 193302 (2003).

[22] A. Fang, Y.C. Chang and J. Tucker, Phys. Rev. B **66**, 155331 (2002).

[23] F. Parisoli, C.J. Wellard, L.C.L. Hollenberg and C.I. Pakes, *15th Aust. Inst. of Phys. Congress,* (Casual Productions, Sydney, 2002).

[24] C. Kittel, *Introduction to Solid State Physics,* (Wiley, New York, 1986).

[25] S.T. Pantelides and C.T. Sah, Phys. Rev. B **10**, 621 (1974).

[26] S.T. Pantelides. Rev. Mod. Phys. **50**, 797 (1978).

[27] I.S. Gradshteyn and I.M. Ryzhik. *Table of Integrals, Series, and Products,* (Academic Press, New York, 2000).

[28] Technology Computer Aided Design modeling package, Integrated Systems Engineering AG, Zurich.

[29] P.Y. Yu and M. Cardona. *Fundamentals of Semiconductors,* (Springer-Verlag, Berlin, 1996).

[30] A. Messiah. *Quantum Mechanics, Vol. 1,* (North-Holland Pub. Co., Amsterdam, 1961).

[31] J.C. Slater *Quantum Theory of Molecules and Solids, Vol. 1* (McGraw Hill Book Company, New York, 1963)